

Entanglement assisted probe of the non-Markovian to Markovian transition in open quantum system dynamics

Chandrashekhara Gaikwad,^{1,*} Daria Kowsari,^{1,2,3,*} Carson Brame,¹ Xingrui Song,¹ Haimeng Zhang,^{2,4} Martina Esposito,⁵ Arpit Ranadive,⁶ Giulio Cappelli,⁶ Nicolas Roch,⁶ Eli M. Levenson-Falk,^{2,3,4} and Kater W. Murch^{1,†}

¹*Department of Physics, Washington University, St. Louis, Missouri 63130, USA*

²*Center for Quantum Information Science and Technology,*

University of Southern California, Los Angeles, California 90089, USA

³*Department of Physics & Astronomy, University of Southern California, Los Angeles, California 90089, USA*

⁴*Ming Hsieh Department of Electrical & Computer Engineering,*

University of Southern California, Los Angeles, California 90089, USA

⁵*CNR-SPIN Complesso di Monte S. Angelo, via Cintia, Napoli 80126, Italy*

⁶*Université Grenoble Alpes, CNRS, Grenoble INP, Institut Néel, 38000 Grenoble, France*

(Dated: January 26, 2024)

We utilize a superconducting qubit processor to experimentally probe the transition from non-Markovian to Markovian dynamics of an entangled qubit pair. We prepare an entangled state between two qubits and monitor the evolution of entanglement over time as one of the qubits interacts with a small quantum environment consisting of an auxiliary transmon qubit coupled to its readout cavity. We observe the collapse and revival of the entanglement as a signature of quantum memory effects in the environment. We then engineer the non-Markovianity of the environment by populating its readout cavity with thermal photons to show a transition from non-Markovian to Markovian dynamics, reaching a regime where the quantum Zeno effect creates a decoherence-free subspace that effectively stabilizes the entanglement between the qubits.

Decoherence is a ubiquitous challenge in quantum technologies. At a microscopic level, decoherence arises from the entanglement of a quantum system with degrees of freedom in its environment. Without access to these degrees of freedom, information about the quantum state is lost [1, 2]. The monotonic reduction in a quantum state's coherence is typically described by the well-known Gorini-Kossakowski-Sudarshan-Lindblad (GKSL) master equation [3, 4] for the system's density operator ρ . In particular, the GKSL master equation is valid under the Born-Markov set of approximations, which assume both weak coupling to the environment, and that the environment is Markovian, i.e. memoryless [5]. This mathematically amenable description is surprisingly effective in describing a broad range of quantum dynamics. Moreover, in the Markovian regime, dissipation engineering by an intentional introduction of Markovian dissipation has been employed as a powerful method of quantum control; with applications including error correction [6–8], state preparation [9, 10], state stabilization [11, 12], and quantum simulation [13]. Naturally, however, there is another paradigm of decoherence known as the non-Markovian regime, where quantum memory effects induced by large system-environment correlations thwart a Markovian description. In this regime, the dynamics of the system is governed by the generalized Nakajima-Zwanzig master equation [14, 15] which incorporates the memory effects of the environment.

Non-Markovian dynamics have the potential to enable novel applications stemming from memory effects in

the environment, such as new approaches towards fault-tolerant quantum computation [16–18], fidelity improvement in the implementation of the teleportation algorithms [19], and coherence preservation [20]. The non-Markovianity of an open quantum system can be measured using two common methods. The most prominent measure is known as the *trace distance* method proposed by Breuer et. al. [21], which relies on the fact that any completely positive trace-preserving (CPTP) quantum map between two-time steps will only result in a decrease of the distinguishability between two quantum states, hence any increase in the distance between states is associated with memory effects [22]. Later, an *entanglement measure* was introduced by Rivas et. al. [23], where one probes quantum memory effects by allowing part of an entangled pair to interact with an environment. Again, a CPTP map will only decrease the degree of entanglement and an increase in entanglement during the system evolution is a signature of quantum memory effects. Both methods [24] have been employed to observe signatures of non-Markovianity, notably in nitrogen-vacancy centers [25–27], photonic systems [28–30], and the trapped ion platform [31].

In this Letter, we harness the entanglement between two superconducting qubits as a probe of quantum memory effects. We initialize the qubits in a Bell state and study the qubits' concurrence [32] over time as one of the qubits interacts with a small quantum environment consisting of a third qubit dispersively coupled to a microwave resonator. We observe collapse and then revival of the qubits' concurrence as a clear signature of the non-Markovian nature of the environment as the qubit becomes entangled and then disentangled with the environment. The non-Markovianity of the environment is then

* Equal contribution

† murch@physics.wustl.edu

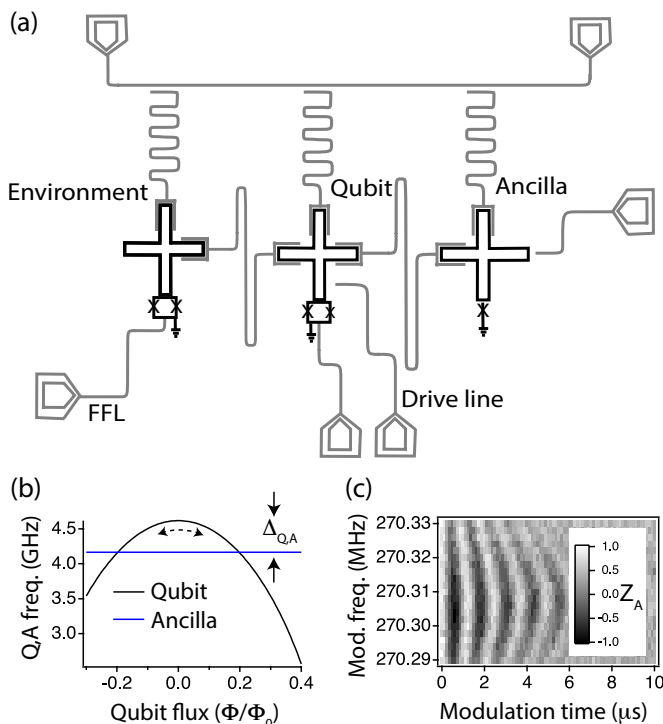


FIG. 1. **Experiment setup.** (a) Sketch of the experiment which includes three qubits respectively labeled “Environment”, “Qubit”, “Ancilla”. The qubits share resonators that mediate nearest-neighbor coupling. Each qubit is coupled to a readout resonator, which can be probed by a common feedline. The Environment and Qubit are frequency tunable via on-chip fast flux lines (FFL). (b) The respective frequencies of the Qubit and Ancilla; resonant coupling between the qubits is achieved by applying a parametric modulation of the Qubit at roughly $\Delta_{Q,A}/2$. (c) When the Qubit is prepared in its excited state, parametric resonance can be observed by examining the Ancilla excitation versus modulation frequency.

tuned by introducing Lindblad dephasing on the environment. This allows us to investigate a non-Markovian-to-Markovian transition in the dynamics. In this non-Markovian regime, we further increase the dissipation on the environment, ultimately reaching a regime where the quantum Zeno effect pins the environment state, thereby preserving the qubits’ entanglement.

Figure 1(a) displays the basic setup of the experiment. The experiment comprises a three-qubit processor with individual readout resonators dispersively coupled to each qubit and nearest-neighbor qubits sharing a resonator mediated coupling. The readout resonators allow us to perform individual state readouts of the three qubits by probing the associated microwave resonators with a microwave drive. We first focus on a sub-portion of the processor with two qubits denoted as the “Qubit” and the “Ancilla”. The Qubit is frequency tunable via a Superconducting QUantum Interference Device (SQUID) loop and the Ancilla is fixed-frequency, both designed to be in the transmon regime [33]. In order to minimize the

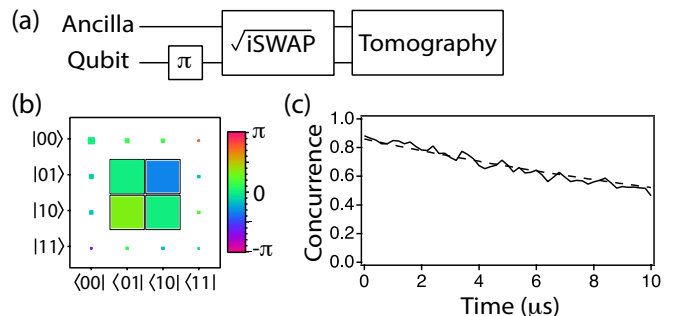


FIG. 2. **Qubit-Ancilla entanglement.** (a) We prepare an entangled state by initializing the Qubit in the excited state, and then applying a \sqrt{i} SWAP gate via parametric modulation. (b) Quantum state tomography allows us to reconstruct the Qubit–Ancilla density operator, yielding an entangled state of the form $\frac{1}{\sqrt{2}}(|10\rangle + e^{i\phi}|01\rangle)$. (c) The measured Qubit–Ancilla concurrence versus time (solid line); we observe a monotonic decrease in the entanglement over time consistent with the single-qubit dephasing rates (dashed line).

decoherence effects from flux noise, we operate the Qubit at its flux sweet spot and introduce coupling to the Ancilla via parametric modulation [34]. To this end, we apply an ac radio frequency drive on the Qubit fast flux line at roughly half the detuning between the Qubit and Ancilla (Fig. 1(b)). We identify the resonance condition between the Qubit and Ancilla by initializing the qubit in its excited state and then applying the parametric modulation for a variable duration. Figure 1(c) shows the time evolution of the Ancilla $\langle\sigma_z\rangle \equiv Z_A$ near the parametric resonance. We observe a clear chevron profile with detuning from which we extract a parametric coupling rate of $\Omega_{Q,A}/2\pi = 0.477$ MHz.

We utilize this parametric coupling to produce a Bell state between the Qubit and Ancilla, as depicted in Fig. 2(a). After applying a π rotation to the Qubit, we activate the parametric coupling for 530 ns, corresponding to a \sqrt{i} SWAP gate, in principle, leaving the Qubit and Ancilla in a state, $\frac{1}{\sqrt{2}}(|10\rangle + e^{i\phi}|01\rangle)$ [35]. We utilize quantum state tomography of the Qubit and Ancilla to characterize the resulting entangled state. For this, we measure 9 Pauli expectation value pairs, $\{\langle\Sigma_Q\Sigma_A\rangle\}$, with $\Sigma_{Q,A} \in \{X, Y, Z\}$ by simultaneously measuring the state of both the Qubit and Ancilla [36]. The average readout fidelities of the Qubit and Ancilla are respectively 0.97 and 0.96. As discussed in the Supplementary Materials, we use a maximum likelihood estimation method [37] to determine the components of the Qubit–Ancilla density matrix, displayed in Fig. 2(b). We observe a Bell state fidelity of 0.91, corresponding to a concurrence of 0.89.

With the Qubit and Ancilla entangled, we now study the evolution of the entanglement over time as the system sits idle. We display the Qubit–Ancilla concurrence versus time in Fig. 2(c). The concurrence slowly decreases over a timescale consistent with the respective individual dephasing times of the Qubit ($T_2^* = 39 \mu\text{s}$) and Ancilla

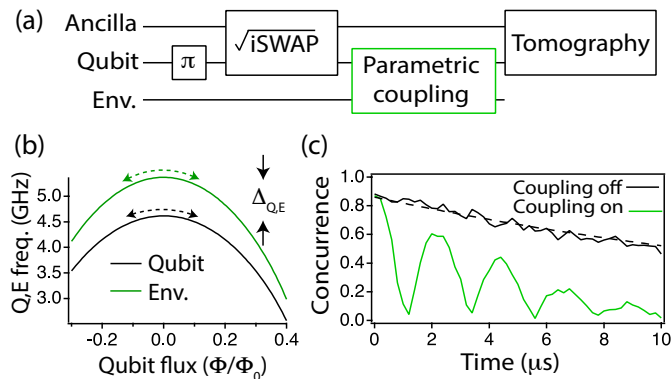


FIG. 3. **Concurrence revival due to non-Markovianity.** (a) We prepare an entangled state between the Qubit and Ancilla, then we apply a parametric coupling between the Qubit and Environment, finally, we perform a set of tomography pulses to reconstruct the density matrix of the Qubit–Ancilla subspace. The concurrence evolution is realized by varying the length of the Qubit–Environment parametric coupling pulses. (b) The respective frequencies of Qubit and Environment showing the Qubit–Environment detuning. (c) Concurrence evolution as a function of the Qubit–Environment parametric coupling pulse length (green). The black curve shows the concurrence evolution when the parametric coupling is turned off.

($T_2^* = 41 \mu\text{s}$), as given by the dashed line in Fig. 2(c).

We now turn to studying the interaction of the Qubit–Ancilla subspace with the Environment. As displayed in Fig. 3(a), after preparing the Qubit–Ancilla in an initial Bell state, we introduce a parametric coupling between the Qubit and Environment. In this case, we apply flux modulation simultaneously to both the Qubit and Environment (Fig. 3(b)) bringing the two into parametric resonance. Both Qubit and Environment are modulated at approximately one-quarter of their detuning ($\Delta_{Q,E}/4 = 2\pi \times 175 \text{ rad./}\mu\text{s}$), which introduces a resonant transverse coupling between the Qubit–Environment pair at a rate of $\Omega_{Q,E} = 2\pi \times 0.473 \text{ rad./}\mu\text{s}$, limited by the resonator-mediated coupling between the pair. After applying the parametric coupling between Qubit and Environment, we perform quantum state tomography on the Qubit–Ancilla subsystem to determine the remaining concurrence.

Figure 3(c) displays the evolution of the concurrence when the interaction between the Qubit and Environment is introduced. In comparison to the monotonic decrease in entanglement observed previously (black curve), we now note a rapid decrease in entanglement, with clear revivals at later times (green curve). The initial decrease is expected from the principle of monogamy of entanglement [38]. Since the Qubit–Ancilla system is in a maximally entangled state, the entanglement between the Qubit–Environment introduced by the parametric coupling must cause the Qubit–Ancilla entanglement to decrease. The revival of entanglement occurs as the Qubit–Environment coupling continues and the Environment state is swapped back into the Qubit. This revival of

entanglement is a clear indicator of non-Markovianity, indicating that the environment has quantum coherent memory. This is indeed expected since the environment is itself a simple two-level system. The non-Markovianity of the system can be calculated as [23],

$$\mathcal{N} = \int_{t_0}^{t_f} dt \left| \frac{d\mathcal{C}[\rho_{Q,A}(t)]}{dt} \right| - \Delta\mathcal{C}, \quad (1)$$

where $\mathcal{C}[\cdot]$ denotes the concurrence measure, $\Delta\mathcal{C}$ is the difference in the concurrence at the initial and final steps of the evolution, and $\rho_{Q,A}$ represents the Qubit–Ancilla density matrix. To elaborate, we look at the time derivative of the concurrence over the entire time evolution of the system $\in [t_0 = 0 \mu\text{s}, t_f = 10 \mu\text{s}]$ at discrete time steps. It is clear from Eq. 1 that the positive slope of the concurrence contributes to the non-Markovianity measure. By applying Eq. 1 to the data in Fig. 3(c), we achieve a non-Markovianity of $\mathcal{N} = 1.4$.

With a clear demonstration of non-Markovian dynamics, we now study how this measure changes as the memory of the Environment is tuned. We achieve this by expanding the size of the Environment to include the quantum states of light that occupy the microwave resonator that is dispersively coupled to the Environment. So far, we have considered this resonator to remain in the vacuum state, which does not affect the Environment’s memory. Now, we introduce pseudo-thermal photons into this resonator via a noisy microwave drive as indicated in Fig. 4(a). The interaction between the Environment and its resonator is captured by the simple dispersive coupling Hamiltonian, $H_{\text{int}} = \chi a^\dagger a \sigma_z^E$, where $\chi/2\pi = 200 \text{ kHz}$ is the dispersive coupling rate, $a^\dagger a$ is the resonator photon number, and σ_z^E is the Pauli operator that acts on the Environment in the energy basis. This interaction can be viewed as either an Environment-state-dependent frequency shift on the resonator frequency, whereby photons carry away information about the state of the Environment, or as an ac-Stark shift of the qubit frequency, whereby the fluctuating intra-resonator photon number dephases the qubit [9, 40].

The noisy drive on the cavity is chosen to have a bandwidth (1.8 MHz) that exceeds χ , ensuring a uniform drive independent of the Environment state. Furthermore, this drive is set to have a correlation time (90 ns) much shorter than any other timescale of the dynamics, allowing us to treat its dephasing effect as Markovian. We calibrate the dephasing via direct Ramsey measurements on the Environment. This establishes a relationship between the dephasing rate and the noise amplitude (A_{in}) as shown in Fig. 4(b). We find an empirical relationship for the Environment dephasing $\gamma = 1.84(\mu\text{s})^{-1} A_{\text{in}}^{1.5}$, as given by the black line in Fig. 4(b).

The introduction of the thermal photons into the Environment causes slight shifts in the parametric coupling between the Qubit and the Environment. As such, we calibrate the parametric coupling between the Qubit and Environment for each value of A_{in} . Figure 4(c) shows the resulting parametric coupling between the Qubit and

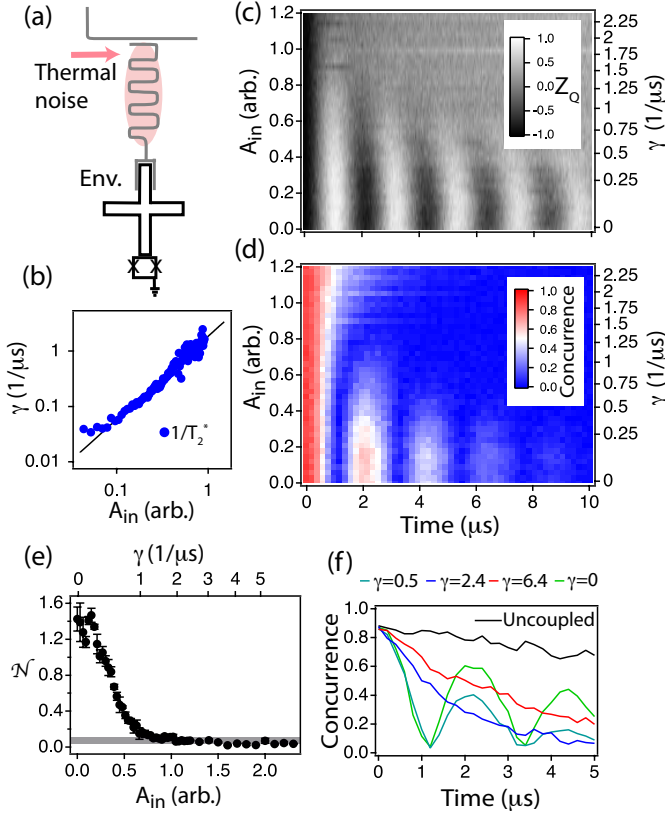


FIG. 4. Non-Markovian to Markovian transition. (a) By driving the Environment’s readout resonator with pseudo-thermal noise of amplitude A_{in} we tune the Environment’s memory. (b) This memory is quantified through Ramsey measurements on the Environment to determine the dephasing rate γ versus A_{in} . (c) For each value of A_{in} we calibrate the frequency of the parametric drive between the Qubit and Environment by studying Z_Q versus time and maximizing the population transfer [39]. (d) The Qubit–Ancilla concurrence versus time for different Environment dephasing rates. The transition to monotonic behavior indicates the transition from non-Markovian to Markovian dynamics. (e) The non-Markovian measure (1) quantified across the transition. The error bars indicate the standard error of the mean from three independent experimental trials. The gray bar indicates the measure applied to the case where the Environment is decoupled and characterizes the background of the measure. (f) The concurrence versus time for a few specific dephasing rates (expressed in units of μs^{-1}).

Environment when the Qubit is initialized in the excited state and the parametric coupling is activated for a variable duration of time. By increasing the dephasing of the Environment, we observe diminished population transfer contrast between the Qubit and the Environment.

Next, we investigate the time evolution of the Qubit–Ancilla concurrence for different values of the Environment dephasing. Increasing the Environment dephasing induces a transition from non-Markovian to Markovian dynamics as displayed in Fig. 4(d). We quantify this transition via the measure (1) as displayed in Fig. 4(e);

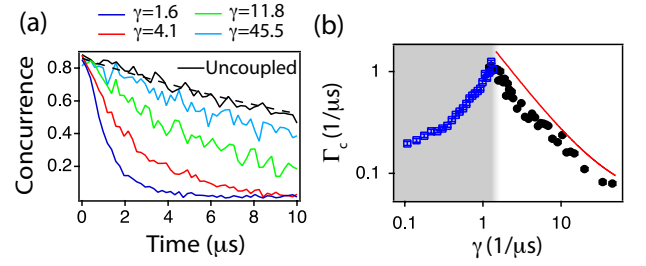


FIG. 5. Quantum Zeno stabilization of entanglement. (a) Qubit–Ancilla concurrence versus time for different Environment dephasing rates; as the dephasing increases, the entanglement approaches the uncoupled case consistently with the Qubit and Ancilla’s individual dephasing rates. (b) The exponential decay rate of the concurrence (Γ_c) versus Environment dephasing rate. The gray region indicates the non-Markovian regime, where we determine Γ_c by fitting the overall (non-monotonic) decay envelope of the concurrence. In the Markovian regime, we observe that the Zeno effect suppresses the concurrence decay induced by the environment, in agreement with the expected scaling (red line).

as the dephasing of the Environment is increased beyond $\gamma \simeq 1 (\mu\text{s})^{-1}$ the dynamics are Markovian.

In Fig. 4(f) we display the concurrence versus time for a few selected values of γ . We note two important trends; first, in the non-Markovian regime, increasing dephasing accelerates the decay envelope of the concurrence (compare $\gamma = 0$ and $\gamma = 0.5$), and second, in the Markovian regime, further increasing dephasing slows the decay of the concurrence ($\gamma = 2.4$ and $\gamma = 6.4$). This can be understood within the context of the quantum Zeno effect [41–47]. The thermal photons perform measurement (at rate γ) of the Environment, which slows the coupling induced by the parametric drive. In Fig. 5, we explore in detail how the dephasing of the Environment affects the Qubit–Ancilla entanglement. Figure 5a displays the concurrence versus time for several values of the dephasing in the Markovian regime. For increasing measurement on the Environment, we see that the decay of concurrence is slowed, approaching the limiting case where the Qubit is completely uncoupled from the Environment. We characterize the exponential decay of the concurrence with a rate Γ_c , and display this rate versus Environment dephasing in Fig. 5b in both the non-Markovian and Markovian regimes; the transition between these two regimes coincides with the onset of Zeno stabilization of the entanglement. Under the standard analysis of the Zeno effect [46, 48], we expect $\Gamma_c = \Omega_{Q,E}^2/4\gamma + \Gamma_0$. Here $\Gamma_0 = 1/T_2^{*Q} + 1/T_2^{*A}$ is the decay rate of the concurrence when the Environment is decoupled. We observe close agreement with this expected scaling (red curve). This demonstrates a new approach to preserving quantum entanglement via Zeno-enabled pinning of environment states.

In conclusion, we have quantified the non-Markovian to Markovian transition with an entanglement-assisted

probe. Importantly, the probe is sensitive to the *quantum memory* of the environment; a classical environment that stores populations will not result in the revival of concurrence for the entangled probe. This approach can have utility in the test of the quantum nature of decoherence channels (e.g. in testing models of quantum gravity [49]). Moreover, by introducing controllable dissipation on the environment we observe stabilization of the Qubit–Ancilla subsystem, highlighting how dissipation forms a powerful tool for quantum subspace engineering [13].

ACKNOWLEDGMENTS

Acknowledgments—The authors are thankful for the useful discussions with Kade Head-Marsden, Patrick Harrington, Weijian Chen, Kaiwen Zheng, Maryam Abbasi, Serra Erdamar, and Archana Kamal. This research was supported by NSF Grants No. PHY-1752844 (CA-REER) and OMA-1936388, the Air Force Office of Scientific Research (AFOSR) Multidisciplinary University Research Initiative (MURI) Award on Programmable systems with non-Hermitian quantum dynamics (Grant No. FA9550-21-1-0202), the John Templeton Foundation, Grant No. 61835, ONR Grant Nos. N00014-21-1-2630 and N00014-21-1-2688 (YIP), Research Corp. Grant No. 27550 (Cottrell), European Union’s FET Open AVaQus grant no. 899561 and Marie Skłodowska-Curie grant no. MSCA-IF-835791. Devices were fabricated and provided by the Superconducting Qubits at Lincoln Laboratory (SQUILL) Foundry at MIT Lincoln Laboratory, with funding from the Laboratory for Physical Sciences (LPS) Qubit Collaboratory.

REFERENCES

- [1] Wojciech Hubert Zurek. Decoherence, einselection, and the quantum origins of the classical. *Rev. Mod. Phys.*, 75:715–775, May 2003.
- [2] Ph. Jacquod and C. Petitjean. Decoherence, entanglement and irreversibility in quantum dynamical systems with few degrees of freedom. *Advances in Physics*, 58(2):67–196, 2009.
- [3] G. Lindblad. On the generators of quantum dynamical semigroups. *Communications in Mathematical Physics*, 48(2):119 – 130, 1976.
- [4] V. Gorini, A. Kossakowski, and E. C. G. Sudarshan. Completely positive dynamical semigroups of N-level systems. *Journal of Mathematical Physics*, 17(5):821–825, 1976.
- [5] H. P. Breuer and F. Petruccione. *The Theory of Open Quantum Systems*. Oxford University Press, 01 2007.
- [6] Christian Kraglund Andersen, Ants Remm, Stefania Lazar, Sebastian Krinner, Nathan Lacroix, Graham J. Norris, Mihai Gabureac, Christopher Eichler, and Andreas Wallraff. Repeated quantum error detection in a surface code. *Nature Physics*, 16(8):875–880, 2020.
- [7] Zaki Leghtas, Gerhard Kirchmair, Brian Vlastakis, Robert J. Schoelkopf, Michel H. Devoret, and Mazyar Mirrahimi. Hardware-Efficient Autonomous Quantum Memory Protection. *Phys. Rev. Lett.*, 111:120501, Sep 2013.
- [8] S. Touzard, A. Grimm, Z. Leghtas, S. O. Mundhada, P. Reinhold, C. Axline, M. Reagor, K. Chou, J. Blumoff, K. M. Sliwa, S. Shankar, L. Frunzio, R. J. Schoelkopf, M. Mirrahimi, and M. H. Devoret. Coherent Oscillations inside a Quantum Manifold Stabilized by Dissipation. *Phys. Rev. X*, 8:021005, Apr 2018.
- [9] K. W. Murch, U. Vool, D. Zhou, S. J. Weber, S. M. Girvin, and I. Siddiqi. Cavity-assisted quantum bath engineering. *Physical Review Letters*, 109(18):1–5, 2012.
- [10] P. Magnard, P. Kurpiers, B. Royer, T. Walter, J.-C. Besse, S. Gasparinetti, M. Pechal, J. Heinsoo, S. Storz, A. Blais, and A. Wallraff. Fast and Unconditional All-Microwave Reset of a Superconducting Qubit. *Phys. Rev. Lett.*, 121:060502, Aug 2018.
- [11] E. T. Holland, B. Vlastakis, R. W. Heeres, M. J. Reagor, U. Vool, Z. Leghtas, L. Frunzio, G. Kirchmair, M. H. Devoret, M. Mirrahimi, and R. J. Schoelkopf. Single-Photon-Resolved Cross-Kerr Interaction for Autonomous Stabilization of Photon-Number States. *Phys. Rev. Lett.*, 115:180501, Oct 2015.
- [12] M. E. Kimchi-Schwartz, L. Martin, E. Flurin, C. Aron, M. Kulkarni, H. E. Tureci, and I. Siddiqi. Stabilizing Entanglement via Symmetry-Selective Bath Engineering in Superconducting Qubits. *Phys. Rev. Lett.*, 116:240503, Jun 2016.
- [13] Patrick M. Harrington, Erich J. Mueller, and Kater W. Murch. Engineered dissipation for quantum information science. *Nature Reviews Physics*, 4(10):660–671, 2022.
- [14] S. Nakajima. On Quantum Theory of Transport Phenomena: Steady Diffusion. *Progress of Theoretical Physics*, 20(6):948–959, 12 1958.
- [15] R. Zwanzig. Ensemble Method in the Theory of Irreversibility. *The Journal of Chemical Physics*, 33(5):1338–1341, 1960.
- [16] Dorit Aharonov, Alexei Kitaev, and John Preskill. Fault-Tolerant Quantum Computation with Long-Range Correlated Noise. *Phys. Rev. Lett.*, 96:050504, Feb 2006.
- [17] Robert Alicki, Daniel A. Lidar, and Paolo Zanardi. Internal consistency of fault-tolerant quantum error correction in light of rigorous derivations of the quantum Markovian limit. *Phys. Rev. A*, 73:052311, May 2006.
- [18] Mirko Rossini, Dominik Maile, Joachim Ankerhold, and Brecht I. C. Donvil. Single-Qubit Error Mitigation by Simulating Non-Markovian Dynamics. *Phys. Rev. Lett.*, 131:110603, Sep 2023.
- [19] Zhao-Di Liu, Yong-Nan Sun, Bi-Heng Liu, Chuan-Feng Li, Guang-Can Guo, Sina Hamedani Raja, Henri Lyyra, and Jyrki Piilo. Experimental realization of high-fidelity teleportation via a non-Markovian open quantum system. *Phys. Rev. A*, 102:062208, Dec 2020.
- [20] Evangelos Vlachos, Haimeng Zhang, Vivek Maurya, Jeffrey Marshall, Tameem Albash, and E. M. Levenson-Falk. Master equation emulation and coherence preservation with classical control of a superconducting qubit. *Phys. Rev. A*, 106:062620, Dec 2022.
- [21] Heinz-Peter Breuer, Elsi-Mari Laine, and Jyrki Piilo. Measure for the Degree of Non-Markovian Behavior of Quantum Processes in Open Systems. *Phys. Rev. Lett.*, 103:210401, Nov 2009.

- [22] Heinz-Peter Breuer, Elsi-Mari Laine, Jyrki Piilo, and Bassano Vacchini. Colloquium: Non-Markovian dynamics in open quantum systems. *Rev. Mod. Phys.*, 88:021002, Apr 2016.
- [23] Ángel Rivas, Susana F. Huelga, and Martin B. Plenio. Entanglement and Non-Markovianity of Quantum Evolutions. *Phys. Rev. Lett.*, 105:050403, Jul 2010.
- [24] P. Haikka, J. D. Cresser, and S. Maniscalco. Comparing different non-Markovianity measures in a driven qubit system. *Phys. Rev. A*, 83:012112, Jan 2011.
- [25] Yang Dong, Yu Zheng, Shen Li, Cong-Cong Li, Xiang-Dong Chen, Guang-Can Guo, and Fang-Wen Sun. Non-Markovianity-assisted high-fidelity Deutsch–Jozsa algorithm in diamond. *npj Quantum Information*, 4(1):3, 2018.
- [26] J. F. Haase, P. J. Vetter, T. Unden, A. Smirne, J. Roskopf, B. Naydenov, A. Stacey, F. Jelezko, M. B. Plenio, and S. F. Huelga. Controllable Non-Markovianity for a Spin Qubit in Diamond. *Phys. Rev. Lett.*, 121:060401, Aug 2018.
- [27] F. Wang, P.-Y. Hou, Y.-Y. Huang, W.-G. Zhang, X.-L. Ouyang, X. Wang, X.-Z. Huang, H.-L. Zhang, L. He, X.-Y. Chang, and L.-M. Duan. Observation of entanglement sudden death and rebirth by controlling a solid-state spin bath. *Phys. Rev. B*, 98:064306, Aug 2018.
- [28] Bi-Heng Liu, Li Li, Yun-Feng Huang, Chuan-Feng Li, Guang-Can Guo, Elsi-Mari Laine, Heinz-Peter Breuer, and Jyrki Piilo. Experimental control of the transition from Markovian to non-Markovian dynamics of open quantum systems. *Nature Physics*, 7(12):931–934, 2011.
- [29] Nadja K. Bernardes, Alvaro Cuevas, Adeline Orioux, C. H. Monken, Paolo Mataloni, Fabio Sciarrino, and Marcelo F. Santos. Experimental observation of weak non-Markovianity. *Scientific Reports*, 5(1):17520, 2015.
- [30] Kang-Da Wu, Zhibo Hou, Guo-Yong Xiang, Chuan-Feng Li, Guang-Can Guo, Daoyi Dong, and Franco Nori. Detecting non-Markovianity via quantified coherence: theory and experiments. *npj Quantum Information*, 6(1):55, 2020.
- [31] M. Gessner, M. Ramm, T. Pruttivarasin, A. Buchleitner, H.-P. Breuer, and H. Häffner. Local detection of quantum correlations with a single trapped ion. *Nature Physics*, 10(2):105–109, 2014.
- [32] William K. Wootters. Entanglement of Formation of an Arbitrary State of Two Qubits. *Phys. Rev. Lett.*, 80:2245–2248, Mar 1998.
- [33] Jens Koch, Terri M Yu, Jay Gambetta, A A Houck, D I Schuster, J Majer, Alexandre Blais, M H Devoret, S M Girvin, and R J Schoelkopf. Charge-insensitive qubit design derived from the Cooper pair box. *Physical Review A*, 76(4):042319, oct 2007.
- [34] Matthew Reagor, Christopher B. Osborn, Nikolas Tezak, Alexa Staley, Guenevere Prawiroatmodjo, Michael Scheer, Nasser Alidoust, Eyob A. Sete, Nicolas Didier, Marcus P. da Silva, Ezer Acala, Joel Angeles, Andrew Bestwick, Maxwell Block, Benjamin Bloom, Adam Bradley, Catvu Bui, Shane Caldwell, Lauren Capelluto, Rick Chilcott, Jeff Cordova, Genya Crossman, Michael Curtis, Saniya Deshpande, Tristan El Bouayadi, Daniel Girshovich, Sabrina Hong, Alex Hudson, Peter Karalekas, Kat Kuang, Michael Lenihan, Riccardo Manenti, Thomas Manning, Jayss Marshall, Yuvraj Mohan, William O’Brien, Johannes Otterbach, Alexander Papageorge, Jean-Philip Paquette, Michael Pelstring, Anthony Polloreno, Vijay Rawat, Colm A. Ryan, Russ Renzas, Nick Rubin, Damon Russel, Michael Rust, Diego Scarabelli, Michael Selvanayagam, Rodney Sinclair, Robert Smith, Mark Suska, Ting-Wai To, Mehrnoosh Vahidpour, Nagesh Vodrahalli, Tyler Whyland, Kamal Yadav, William Zeng, and Chad T. Rigetti. Demonstration of universal parametric entangling gates on a multi-qubit lattice. *Science Advances*, 4(2), February 2018.
- [35] S. A. Caldwell, N. Didier, C. A. Ryan, E. A. Sete, A. Hudson, P. Karalekas, R. Manenti, M. P. da Silva, R. Sinclair, E. Acala, N. Alidoust, J. Angeles, A. Bestwick, M. Block, B. Bloom, A. Bradley, C. Bui, L. Capelluto, R. Chilcott, J. Cordova, G. Crossman, M. Curtis, S. Deshpande, T. El Bouayadi, D. Girshovich, S. Hong, K. Kuang, M. Lenihan, T. Manning, A. Marchenkov, J. Marshall, R. Maydra, Y. Mohan, W. O’Brien, C. Osborn, J. Otterbach, A. Papageorge, J.-P. Paquette, M. Pelstring, A. Polloreno, G. Prawiroatmodjo, V. Rawat, M. Reagor, R. Renzas, N. Rubin, D. Russell, M. Rust, D. Scarabelli, M. Scheer, M. Selvanayagam, R. Smith, A. Staley, M. Suska, N. Tezak, D. C. Thompson, T.-W. To, M. Vahidpour, N. Vodrahalli, T. Whyland, K. Yadav, W. Zeng, and C. Rigetti. Parametrically Activated Entangling Gates Using Transmon Qubits. *Phys. Rev. Appl.*, 10:034050, Sep 2018.
- [36] Suman Kundu, Nicolas Gheeraert, Sumeru Hazra, Tanay Roy, Kishor V. Salunkhe, Meghan P. Patankar, and R. Vijay. Multiplexed readout of four qubits in 3D circuit QED architecture using a broadband Josephson parametric amplifier. *Applied Physics Letters*, 114(17):172601, 05 2019.
- [37] Daniel F. V. James, Paul G. Kwiat, William J. Munro, and Andrew G. White. Measurement of qubits. *Phys. Rev. A*, 64:052312, Oct 2001.
- [38] Valerie Coffman, Joydip Kundu, and William K. Wootters. Distributed entanglement. *Phys. Rev. A*, 61:052306, Apr 2000.
- [39] In the Supplemental Materials we provide further details on the experimental setup, calibration of the parametric drive, device design, and quantum state tomography. The Supplemental Material contains additional references: [50–55].
- [40] M. Hatridge, S. Shankar, M. Mirrahimi, F. Schackert, K. Geerlings, T. Brecht, K. M. Sliwa, B. Abdo, L. Frunzio, S. M. Girvin, R. J. Schoelkopf, and M. H. Devoret. Quantum Back-Action of an Individual Variable-Strength Measurement. *Science*, 339(6116):178–181, 2013.
- [41] P. M. Harrington, J. T. Monroe, and K. W. Murch. Quantum Zeno Effects from Measurement Controlled Qubit-Bath Interactions. *Physical Review Letters*, 118(24):1–5, 2017.
- [42] B. Misra and E. C. G. Sudarshan. The Zeno’s paradox in quantum theory. *Journal of Mathematical Physics*, 18(4):756–763, 1977.
- [43] Wayne M. Itano, D. J. Heinzen, J. J. Bollinger, and D. J. Wineland. Quantum Zeno effect. *Physical Review A*, 41(5):2295–2300, March 1990.
- [44] K. Kakuyanagi, T. Baba, Y. Matsuzaki, H. Nakano, S. Saito, and K. Semba. Observation of quantum Zeno effect in a superconducting flux qubit. *New Journal of Physics*, 17(6):63035, 2015.
- [45] S. Hacothen-Gourgy, L. P. García-Pintos, L. S. Martin,

- J. Dressel, and I. Siddiqi. Incoherent Qubit Control Using the Quantum Zeno Effect. *Physical Review Letters*, 120(2), January 2018.
- [46] E. Blumenthal, C. Mor, A. A. Diringer, L. S. Martin, P. Lewalle, D. Burgarth, K. B. Whaley, and S. Hacohe-Gourgy. Demonstration of universal control between non-interacting qubits using the Quantum Zeno effect. *npj Quantum Information*, 8(1), July 2022.
- [47] D H Slichter, C Müller, R Vijay, S J Weber, A Blais, and I Siddiqi. Quantum Zeno effect in the strong measurement regime of circuit quantum electrodynamics. *New Journal of Physics*, 18(5):053031, May 2016.
- [48] Jay Gambetta, Alexandre Blais, M. Boissonneault, A. A. Houck, D. I. Schuster, and S. M. Girvin. Quantum trajectory approach to circuit QED: Quantum jumps and the Zeno effect. *Phys. Rev. A*, 77:012112, Jan 2008.
- [49] Eissa Al-Nasrallah, Saurya Das, Fabrizio Illuminati, Luciano Petruzzello, and Elias C. Vagenas. Discriminating quantum gravity models by gravitational decoherence. *Nuclear Physics B*, 992:116246, July 2023.
- [50] Arpit Ranadive, Martina Esposito, Luca Planat, Edgar Bonet, Cécile Naud, Olivier Buisson, Wiebke Guichard, and Nicolas Roch. Kerr reversal in Josephson metamaterial and traveling wave parametric amplification. *Nature Communications*, 13(1):1737, 2022.
- [51] Priti Ashvin Shah, Zlatko Minev, Jeremy Drysdale, Marco Facchini, grace-harper ibm, Thomas G McConkey, Dennis Wang, Yehan Liu, Nick Lanzillo, Will Shanks, Helena Zhang, cdelnano, Matthew Treinish, Abeer Vaishnav, John L Blair, Sagarika Mukesh, ismiria, Christopher Warren, Patrick J. O'Brien, Figen YILMAZ, Clark Miyamoto, Sharky, Samarth Hawaldar, Jagatheesan Jack, PatrickSJacobs, Christian Kraglund Andersen, Eric Arellano, Niko Savola, Paul Nation, and bashensen. qiskit-community/qiskit-metal: Qiskit Metal 0.1.5a1 (2023), June 2023.
- [52] R. Barends, J. Kelly, A. Megrant, D. Sank, E. Jeffrey, Y. Chen, Y. Yin, B. Chiaro, J. Mutus, C. Neill, P. O'Malley, P. Roushan, J. Wenner, T. C. White, A. N. Cleland, and John M. Martinis. Coherent Josephson Qubit Suitable for Scalable Quantum Integrated Circuits. *Phys. Rev. Lett.*, 111:080502, Aug 2013.
- [53] Zlatko K. Minev, Zaki Leghtas, Philip Reinhold, Shantanu O. Mundhada, Asaf Diringer, Daniel Cohen Hillel, Dennis Zi-Ren Wang, Marco Facchini, Priti Ashvin Shah, and Michel Devoret. pyEPR: The energy-participation-ratio (EPR) open-source framework for quantum device design, May 2021. <https://github.com/zlatko-minev/pyEPR> <https://pyepr-docs.readthedocs.io/en/latest/>.
- [54] D. S. Wisbey, A. Martin, A. Reinisch, and J. Gao. New Method for Determining the Quality Factor and Resonance Frequency of Superconducting Micro-Resonators from Sonnet Simulations. *Journal of Low Temperature Physics*, 176(3):538–544, 2014.
- [55] Pauli Virtanen, Ralf Gommers, Travis E. Oliphant, Matt Haberland, Tyler Reddy, David Cournapeau, Evgeni Burovski, Pearu Peterson, Warren Weckesser, Jonathan Bright, Stéfan J. van der Walt, Matthew Brett, Joshua Wilson, K. Jarrod Millman, Nikolay Mayorov, Andrew R. J. Nelson, Eric Jones, Robert Kern, Eric Larson, C J Carey, İlhan Polat, Yu Feng, Eric W. Moore, Jake VanderPlas, Denis Laxalde, Josef Perktold, Robert Cimrman, Ian Henriksen, E. A. Quintero, Charles R. Har-
- ris, Anne M. Archibald, Antônio H. Ribeiro, Fabian Pedregosa, Paul van Mulbregt, and SciPy 1.0 Contributors. SciPy 1.0: Fundamental Algorithms for Scientific Computing in Python. *Nature Methods*, 17:261–272, 2020.

Supplemental Information for “Entanglement assisted probe of the non-Markovian to Markovian transition in open quantum system dynamics”

I. CALIBRATION OF THE QUBIT-ENVIRONMENT PARAMETRIC COUPLING

When the Environment is subject to the additional dissipation channel formed by probing its readout resonator with pseudo-thermal drive, this additional dissipation affects the parametric resonance between the Qubit and Environment. As such, we calibrate the coupling for every value of the noise amplitude. Figure 6 details this calibration. The pseudo-thermal drive on the Environment resonator is generated by frequency modulating a monochromatic tone with Gaussian noise from a function generator. The spectrum of the resulting noise is displayed in Fig. 6(a). Figure 6 (b) displays the spectroscopy of the parametric coupling for different noise amplitudes. We prepare the Qubit in the excited state and measure the Environment excitation probability as a function of the parametric drive applied to both the Qubit and the Environment. For appreciable noise amplitude, the resonance is characteristic of a thermal distribution, Fig. 6(c). By fitting these resonances, we determine the FWHM linewidth. In Fig. 6(d), we compare the additional broadening observed in the parametric resonance (calculated as $8\pi \times \text{FWHM}$, since both the Qubit and Environment are modulated at their flux sweet-spots), to the Environment dephasing rate measured in Fig. 4(b). We observe similar scaling of the dephasing with noise amplitude. Overall, the clean behavior of the parametric coupling, even at very high values of the Environment dephasing, indicates that the parametric drive still functions in the presence of the additional drive on the Environment’s resonator.

II. EXPERIMENTAL SETUP

Figure 7 shows the cryogenic setup of the experiment. The device is packaged in a copper box and surrounded by an additional copper can as well as a Cryoperm shielding to protect the device from infrared radiation and external magnetic fields. The device is further thermalized to the mixing chamber stage via a copper plate. The coaxial

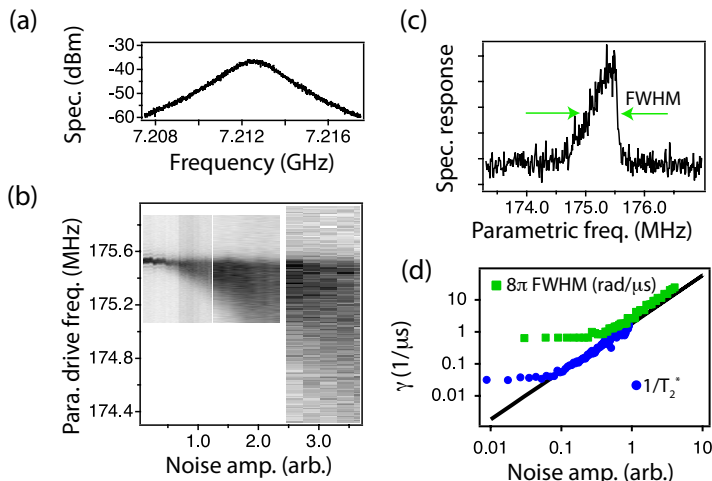


FIG. 6. **Qubit–Environment parametric resonance in the presence of pseudo-thermal noise.** (a) The spectrum of the microwave drive applied at the Environment readout resonator frequency. (b) Spectroscopy of the parametric resonance as given by the Environment excitation probability for different values of the noise amplitude. (c) The observed spectra are asymmetric as is expected from a thermal photon distribution in the cavity. We determine the FWHM of the resonance as an additional measure of the Environment dephasing rate. (d) The parametric resonance bandwidth (scaled to comparable units for the dephasing rate) versus noise amplitude in comparison to the Environment dephasing rate from Fig. 4 (b). This shows that the scaling of the Environment dephasing continues for larger ranges of the noise amplitude than can be probed with Ramsey measurements.

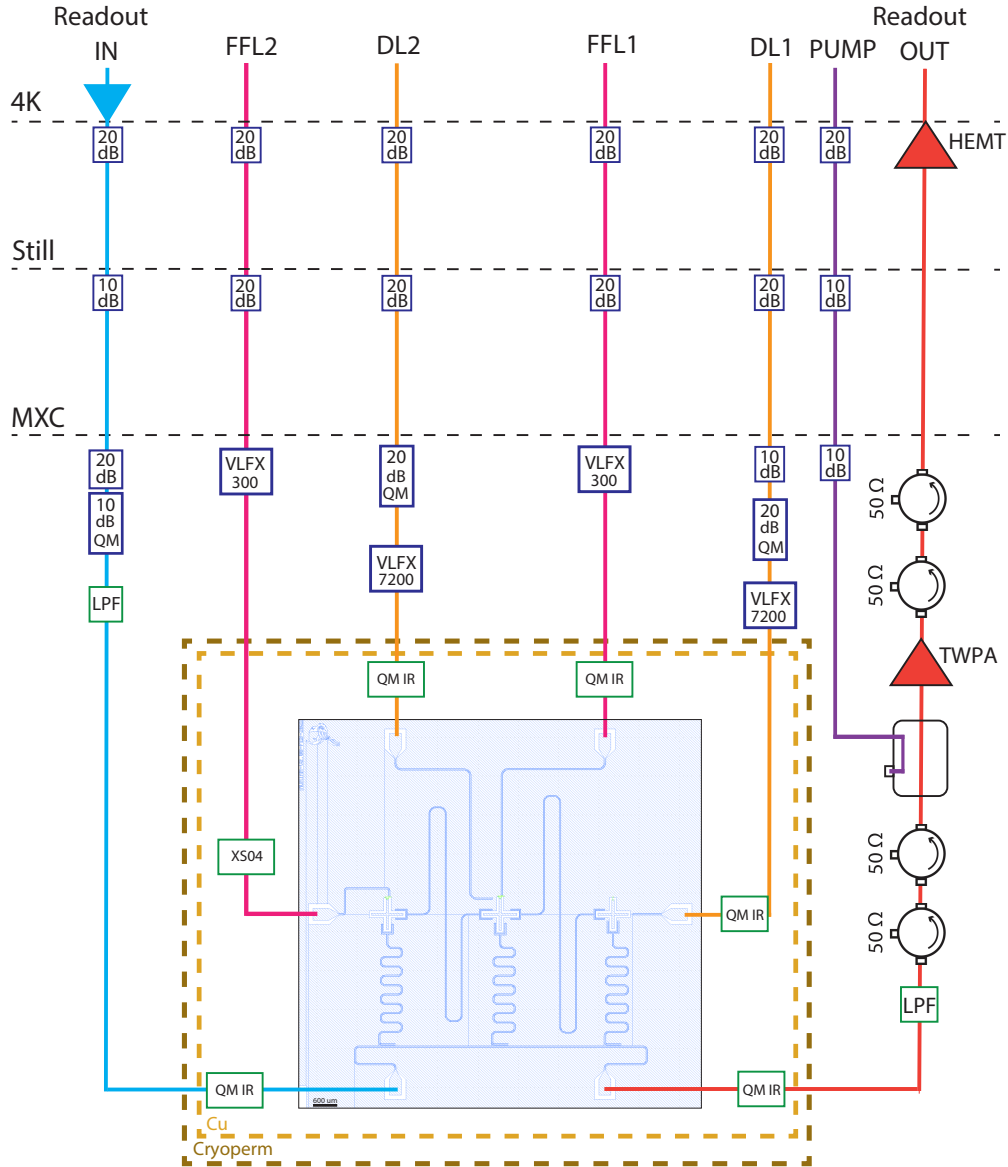


FIG. 7. Cryogenic setup of the experiment.

lines are thermalized via cryogenic microwave attenuators. Note that, the very last attenuators are specific cryogenic attenuators (QMC-CRYOATTF).

For the fast flux lines (FFL), we used a total of 40 dB attenuation as well as 300 MHz low-pass filters (MiniCircuits 300 VLFX) to suppress the high-frequency noise, with a bias-tee at the top of the fridge to apply a DC current to tune the frequency of the qubits. The drive lines DL1 and DL2 have different values of attenuation (70 dB and 60 dB) to account for respective differences in their on-chip coupling. This arrangement of the attenuators allows us to achieve Rabi oscillations as fast as 20 MHz. In addition, we installed 7.2 GHz low-pass filters (MiniCircuits 7200+ VLFX) to mitigate high-frequency noise. Finally, for the readout input line, we added 60 dB of attenuation with a KNL low-pass filter (LPF) at 8 GHz (4L250-7344/T12000-O/O). An Eccosorb infrared filter [labeled QM IR (QMC-CRYOIRF-002MF), or XS04 (an equivalent element)] was installed for every single microwave line inside the copper shielding with > 10 GHz cutoff frequencies to absorb the infrared radiation.

To amplify the output signal, we use a high-electron-mobility transistor (HEMT) low-noise amplifier at the 4K stage as well as a traveling-wave parametric amplifier (TWPA) at milliKelvin temperatures with gains of about 40 dB and 20 dB, respectively. The TWPA used in this experiment is based on the SNAIL architecture resulting in reversed Kerr phase matching [50] with bandwidths as high as 4 GHz and noise temperatures of about 300 mK. The

	$\omega_q/2\pi$ (GHz)	$ \alpha /2\pi$ (MHz)	$\chi_{qc}/2\pi$ (kHz)	$\omega_c/2\pi$ (GHz)	$\kappa/2\pi$ (kHz)	T_1 (μ s)	T_2^* (μ s)
Ancilla	4.6 [4.2]	195 [212]	210 [230]	7.15 [6.94]	200 [270]	[32]	[41]
Qubit	5.1 [4.65]	175 [180]	210 [250]	7.3 [7.09]	200 [206]	[31]	[39]
Env.	5.6 [5.37]	180 [140]	200 [265]	7.47 [7.21]	200 [170]	[28]	[38]

TABLE I. Simulated [measured] parameters of the device used in the experiment.

other advantage of this type of TWPA is that it can be pumped at frequencies ~ 2 GHz away from the range of interest through a directional coupler, which results in minimal interference between the pump and readout signal in the experiment.

III. DEVICE DESIGN AND SIMULATIONS

The device layout is designed using the Qiskit Metal package [51] by incorporating the prominent Xmon qubit geometry [52]. The layout is then imported to the Ansys software in order to perform the finite-element simulations utilizing the eigenmode solver. The simulation results are then imported to the energy-participation quantization package [53] to extract the qubits' frequencies (ω_q) and anharmonicities (α) as well as the readout resonators' frequencies (ω_c) and qubit-cavity dispersive shifts (χ_{qc}). Moreover, the linewidth of the resonators (κ) is estimated using the HFSS-driven modal scattering simulations after employing the 3-dB method [54] to the scattering transmission profile (S_{12}) from the simulations. Table I shows the simulated parameters of the device used in the experiment with the measured values written in brackets, indicating an accuracy of 90% between simulations and measurements. Additionally, the Ancilla-Qubit and Qubit-Environment mediating resonators' frequencies are designed to be 8.0 and 8.6 GHz, respectively.

IV. TWO-QUBIT STATE TOMOGRAPHY

The density matrix of two qubits can be reconstructed by performing 9 distinct measurements. As an example, if our system is prepared in an arbitrary state in the $\{00, 01, 10, 11\}$ basis as, $|\psi\rangle = a|00\rangle + b|01\rangle + c|10\rangle + d|11\rangle$, the $\langle ZZ \rangle$ expectation value can be written as,

$$\begin{aligned} \langle ZZ \rangle &= \frac{\langle \psi | \sigma_z \otimes \sigma_z | \psi \rangle}{\langle \psi | \psi \rangle} = \frac{|a|^2 - |b|^2 - |c|^2 + |d|^2}{|a|^2 + |b|^2 + |c|^2 + |d|^2} \\ &= \frac{\text{pr}^{(z)}(00) - \text{pr}^{(z)}(01) - \text{pr}^{(z)}(10) + \text{pr}^{(z)}(11)}{\text{pr}^{(z)}(00) + \text{pr}^{(z)}(01) + \text{pr}^{(z)}(10) + \text{pr}^{(z)}(11)}, \end{aligned}$$

where σ_z is the Pauli z -matrix and $\text{pr}^{(z)}(00)$ denotes the probability of finding both qubits in their ground states measured along the Z axis. This is achievable by employing a simultaneous heterodyne readout scheme, where we multiplex the readout signal by sending two pulses simultaneously with different intermediate frequencies to track the state of the qubits. A similar approach can be used to measure the rest of the expectation values by applying 9 various combinations of the tomography pulses. Table II includes the required rotation pulse combinations and the corresponding expectation values that can be calculated from each measurement, ignoring the trivial $\langle \mathbb{I} \rangle$.

Having all the 16 expectation values allows us to reconstruct the full density matrix following these steps:

1. Define a lower-triangular matrix as,

$$T = \begin{pmatrix} t_1 & 0 & 0 & 0 \\ t_5 + it_6 & t_2 & 0 & 0 \\ t_7 + it_8 & t_9 + it_{10} & t_3 & 0 \\ t_{11} + it_{12} & t_{13} + it_{14} & t_{15} + it_{16} & t_4 \end{pmatrix},$$

with the density matrix constructed as $\rho = \frac{T^\dagger T}{\text{Tr}(T^\dagger T)}$. This assures the Hermiticity of ρ as well as its trace-normalization.

Rotation	Measurement operator	Expectation values
$R_Y^{\pi/2} \otimes R_Y^{\pi/2}$	XX	$\langle IX \rangle, \langle XI \rangle, \langle XX \rangle$
$R_Y^{\pi/2} \otimes R_X^{-\pi/2}$	XY	$\langle IY \rangle, \langle XI \rangle, \langle XY \rangle$
$R_Y^{\pi/2} \otimes \mathcal{I}$	XZ	$\langle IZ \rangle, \langle XI \rangle, \langle XZ \rangle$
$R_X^{-\pi/2} \otimes R_Y^{\pi/2}$	YX	$\langle IX \rangle, \langle YI \rangle, \langle YX \rangle$
$R_X^{-\pi/2} \otimes R_X^{-\pi/2}$	YY	$\langle IY \rangle, \langle YI \rangle, \langle YY \rangle$
$R_X^{-\pi/2} \otimes \mathcal{I}$	YZ	$\langle IZ \rangle, \langle YI \rangle, \langle YZ \rangle$
$\mathcal{I} \otimes R_Y^{\pi/2}$	ZX	$\langle IX \rangle, \langle ZI \rangle, \langle ZX \rangle$
$\mathcal{I} \otimes R_X^{-\pi/2}$	ZY	$\langle IY \rangle, \langle ZI \rangle, \langle ZY \rangle$
$\mathcal{I} \otimes \mathcal{I}$	ZZ	$\langle IZ \rangle, \langle ZI \rangle, \langle ZZ \rangle$

TABLE II. **Two-qubit tomography measurement operators and their corresponding 16 expectation values.**

2. Construct a minimization vector in the form of, $\mathcal{L}_k = \left(\text{Tr}(\hat{\mathcal{M}}_k \rho) - p_k \right)^2$, where $\hat{\mathcal{M}}_k$ represents the measurement operators (shown in Table II) with p_k being the outcome of each measurement and k runs over all the 16 measurement values.
3. Employ the least_squares function under the scipy.optimize package [55] to minimize the vector defined in step 2 to extract the optimized values for the T matrix elements and reconstruct the density matrix.

The steps above form the well-known maximum likelihood estimation method, which results in high accuracy in reconstructing the full state of the qubits [37].
